ELSEVIER

Ceramics International 25 (1999) 61–67

CERAMICS INTERNATIONAL

Thermal shock resistance of carbon–carbon (C/C) composite by laser irradiation technique

Shigeyasu Amada [a,*], Wu Yi Nong [a], Qi Zhu Min [a], Shigeru Akiyama [b]

[a] *Gunma University, 1-5-1, Tenjin, Kiryu, Gunma, 376-8515 Japan*
[b] *Ship Research Institute, 6-38-1, Shinkawa, Mitaka, Tokyo, 181 Japan*

Received 2 May 1997; accepted 19 November 1997

Abstract

Thermal shock strength of carbon–carbon composite has not been evaluated yet. This paper presents it by laser irradiation technique newly developed for ceramics. Traditionally adapted quenching test has a big difficulty in which heat transfer coefficient is very unstable under the quenching process. To avoid this problem, laser irradiation method was proposed and applied effectively to several ceramics. Thermal shock strength of carbon–carbon composite was evaluated by laser irradiation method and the critical laser power density which causes the material's fracture was obtained. It was concluded that the critical power density can be a new measure to evaluate thermal shock strength.

1. Introduction

Carbon–carbon (C/C) composite has heat-, water- and probably thermal shock-resistant, high strength at elevated temperature, low density and size stability and so on. It is most expected to apply to the components operating under severe temperature circumstances like rockets and space planes. Taking into consideration the material's oxidization problem [1] at high temperature and its properties depending on the manufacturing process [2] and fibre texture [3], C/C composite is still under development. Although their various mechanical properties have been reported [4,5], thermal shock resistance has not been evaluated yet. There is one related report that their strength increases after adding thermal shock on materials [6].

Thermal shock strength of ceramics are traditionally evaluated by quenching technique and by the Hasselman plot to obtain the residual strength [7,8]. Since heat transfer in the quenching process of hot specimens in cold liquid is very unstable, the accuracy of their evaluation was criticized by several researchers [9,10]. To make this problem clear, heat transfer coefficient in the quenching process was precisely measured [11]. New evaluation techniques have been proposed by Faber et al. [12], Lamon and Pherson [13], Takatsu et al. [14] and Awaji [15] in order to avoid this unstable process. And also a new and simple technique with laser irradiation was proposed and applied to several ceramic materials [16–18].

This report presents the evaluation of thermal shock strength of C/C composite based on the laser irradiation technique. Irradiating a laser pulse on the specimen surface, its fracture is sensed by AE (Acoustic Emission) signal. Assuming that the critical power density of laser is defined by the one which causes the specimen's fracture, it can be a new measure to evaluate thermal shock strength. Transient heat conduction and thermal stress analysis are carried out by FEM. Assuming that fracture is initiated by the generated stress beyond the material's strength, critical fracture curve is derived which can map the fracture and non-fracture regions for given laser power density and beam diameter. Finally thermal shock experiments are done by CO_2 laser and prove the appropriateness of the theoretical, critical fracture curve.

2. Carbon–carbon composite

Figs. 1 (a) and (b) show the weaving pattern in plane and cross section, and layer-like structure of the material.

* Corresponding author. Tel.: +81-0277-30-1549, fax: +81-0277-30-1553, e-mail: amanda@cc.gunma-u.ac.jp

0272-8842/98/$—see front matter
PII: S0272-8842(98)00002-9

One thread is spun of about 1000 carbon short fibres. Overall volume fraction of carbon fibres is 40%. The properties of the C/C composite listed in Table 1. The SEM photograph of the fibre texture in C/C composite is shown Fig. 2.

3. Heat conduction and thermal stress analysis by FEM

The C/C composite has a three dimensional structure as shown in Fig. 1. Exactly speaking, three dimensional structural model must be adopted. Since the FEM analysis plays a role of a side support to this evaluation system, we adopted a simple, homogeneous and axially symmetric solid model, so called the 1st approximation model. This model seems to be sufficient to support the proposed evaluation system.

Assuming non-coupled and pseudo-steady state theory, the transient heat conduction and thermal stress analysis are carried out by FEM (MARC Program) for a model as shown in Fig. 3. A cylinder model has a size of diameter $d=50$ mm and height $H=20$ mm which simulates approximately an experimental specimen. Its upper surface is irradiated by laser pulse with beam diameter D, power density P W mm^{-2} of constant distribution and duration 1 s.

Fig. 4 shows the boundary conditions for heat conduction and thermal stress analysis. In heat conduction process, heat is transferred from hot specimen to ambient cold air by heat transfer process whose coefficients are listed in the lower lines of Table 2 [19].

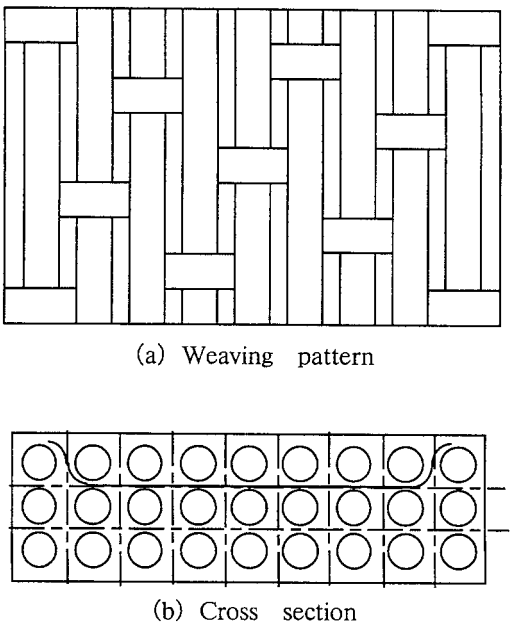

Fig. 1. Weaving pattern.

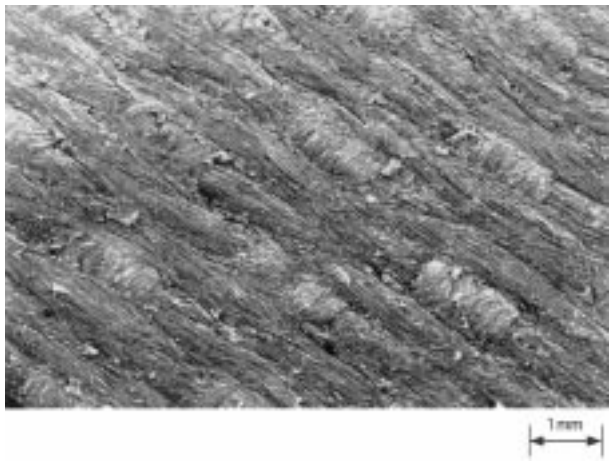

Fig. 2. Surface SEM photograph of C/C composite specimen.

Table 1
Properties of C/C composite

Density	1.4×10^3 (kg m^{-3}
Thermal expansion coefficient	5×10^{-6}(/K)
Heat conductivity	5.2(W/m・K)
Specific heat	0.84(kj/kg・K)
Tensile strength	29.6(Mpa)
Young's modulus	45.11(Gpa)
Poisson's ratio	0.25
Emmisivity (: 10.6μm)	0.90
Heat transfer coefficient (W/m^2・K)	
Upper surface	$h_1=1.32(\Delta T/\ell)^{1/4}$
Vertical side	$h_2=1.42(\Delta T/\ell)^{1/4}$
Bottom surface	$h^3=0.61(\Delta T/\ell)^{1/4}$

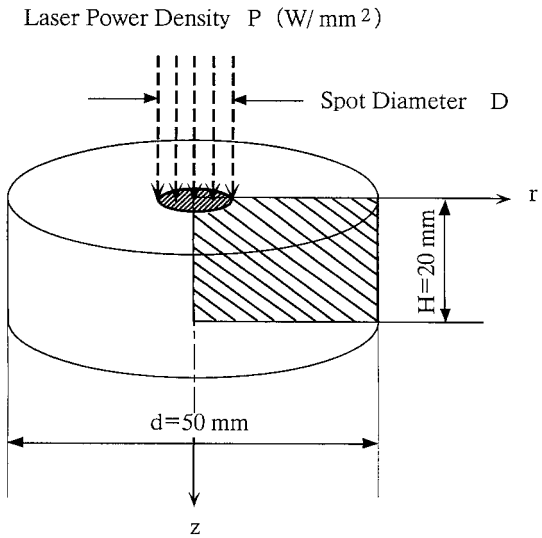

Fig. 3. Analytical model of specimen.

The origin of co-ordinate is fixed at the centre of laser beam on the specimen surface. Let r be radius and z be depth. An element model with arbitrary quadrilateral axisymmetric ring model is used for FEM computations. The total number of elements and nodes are 2150 and 6645, respectively.

4. Distributions of calculated temperature and thermal stress

Fig. 5 shows the temperature distribution on the irradiated surface with respect to r for $P = 2.42\ \mathrm{W\,mm^{-2}}$ at 1 s. The maximum temperature at irradiated centre increases with D and saturates beyond $D = 30$ mm. In that range temperature gives constant distribution within beam. Fig. 6 shows the temperature distribution in the z-coordinate at the various radii for $P = 3\ \mathrm{W\,rnm^{-2}}$, $D = 10$ mm at $t = 1$ s. Temperature does not increase below depth $z = 5$ mm and outside $r = 15$ mm.

Thermal stresses are computed based on the obtained temperature data. Fig. 7 shows the radial stress σ_r distribution on the irradiated surface on the radial direction for $P = 2.4\ \mathrm{W\,mm^{-2}}$ at 1 s. It has the large compressive stress at the centre and asymptotically zero toward the outer periphery. The maximum compressive stress at the centre reaches its highest value for $D = 40$ mm and decreases beyond that beam diameter.

Fig. 8 shows the calculated hoop stress σ_θ distribution on the irradiated surface in the radial direction for the same condition as Fig. 7. It is noted that under axially symmetric state the relation $\sigma_\theta = \sigma_r$ is held at the centre. The large compressive stress is generated at centre, it decreases with radius and changes from compressive to tensile crossing the beam periphery. The largest tensile stress takes place around $r = 5\sim8$ mm out of the beam periphery. Assuming that fracture occurs when the largest tensile stress reaches the value beyond the material strength, crack can be initiated at the place around $r = 5\sim8$ mm where the largest tensile stress occurs. The largest tensile stress increases with D.

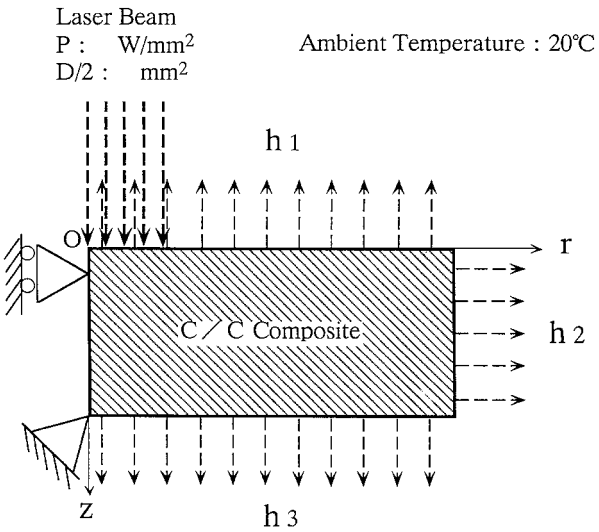

Fig. 4. Boundary conditions of computations.

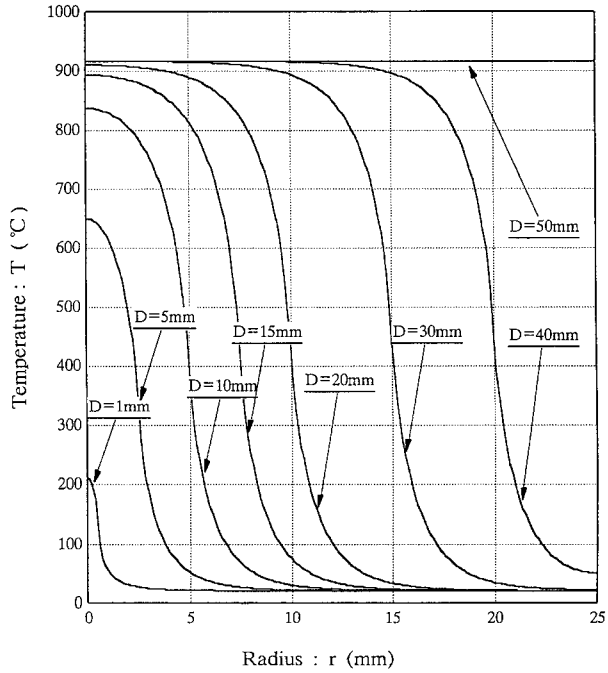

Fig. 5. Temperature distribution on irradiated surface.

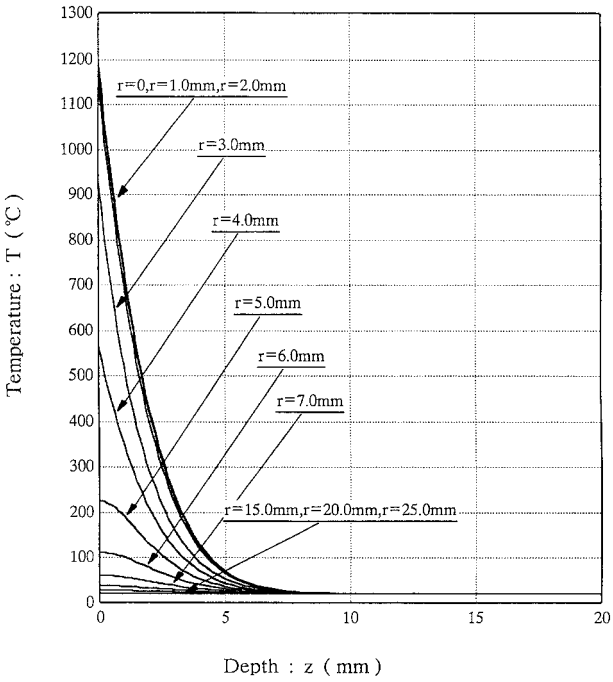

Fig. 6. Temperature distribution along depth.

Fig. 9 shows the radial stress distribution at the centre with respect to depth z. The largest compressive stress is generated on the irradiated surface and changes from compressive to tensile with increase of z. The largest tensile stress arises in the neighbourhood of $z = 6.2$ mm and its value is slightly less than the largest hoop stress on the irradiated surface.

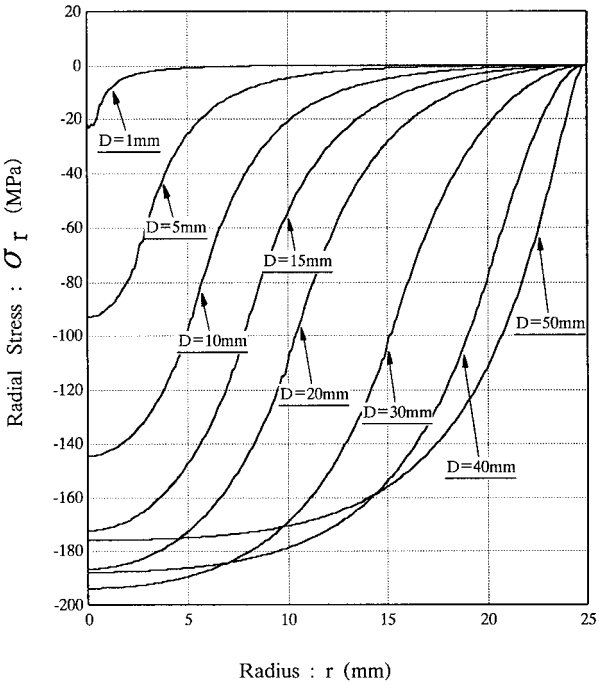

Fig. 7. Radial stress on irradiated surface.

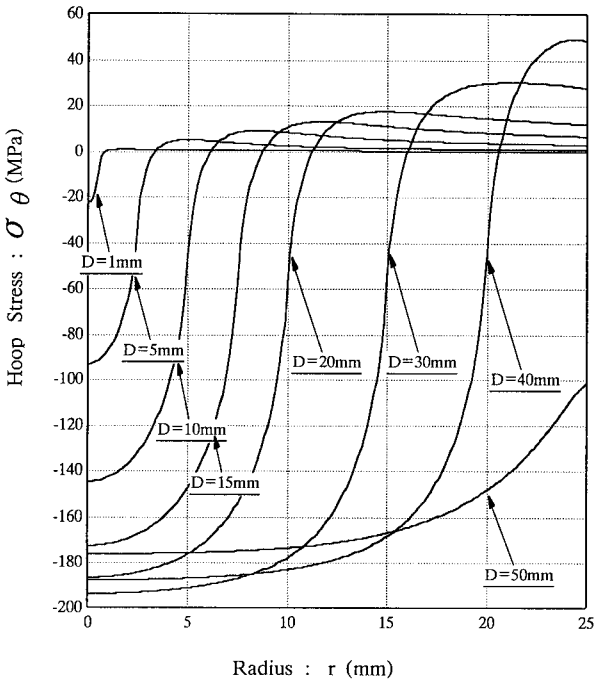

Fig. 8. Hoop stress on irradiated surface.

5. Critical fracture curve of thermal shock

Changing laser power density $1 \sim 25\,\mathrm{W\,mm^{-2}}$, the relation between the largest tensile stress and beam diameters is shown in Fig. 10 for various power densities. The critical power density P_c is defined by the power density under which C/C composite is fractured. Drawing a horizontal straight line at the stress 29.62 MPa in Fig. 10, the crossing points at each curve give the critical power density for beam diameter D.

The relationship between P_c and D leads to a critical fracture curve as shown in Fig. 11. This curve can give an estimation of the critical power density to cause fracture of C/C composite for a given beam diameter D. It was concluded that P_c can be a measure for thermal shock strength of materials. Initially P_c decreases rapidly, its decreasing rate becomes gradually low with D and finally asymptotically approaches to constant value. Predicting this asymptotic value from the critical fracture curve, it is $P_c = 2.0\,\mathrm{W\,mm^{-2}}$ which is rather low as compared with $P_c = 2.9\,\mathrm{W\,mm^{-2}}$ for $A1_2O_3$, $16.5\,\mathrm{W\,mm^{-2}}$ for TiB_2 and $5.2\,\mathrm{W\,mm^{-2}}$ for MACOR (Machinable Ceramics). This is reasoned by that the thread of the used C/C composite is a bundle of the carbon fibres in short length and its tensile strength is rather low.

6. Thermal shock experiments

Fig. 12 shows the adapted system for the experiment. A pulse (duration 1 s) of CO_2 laser with the maximum

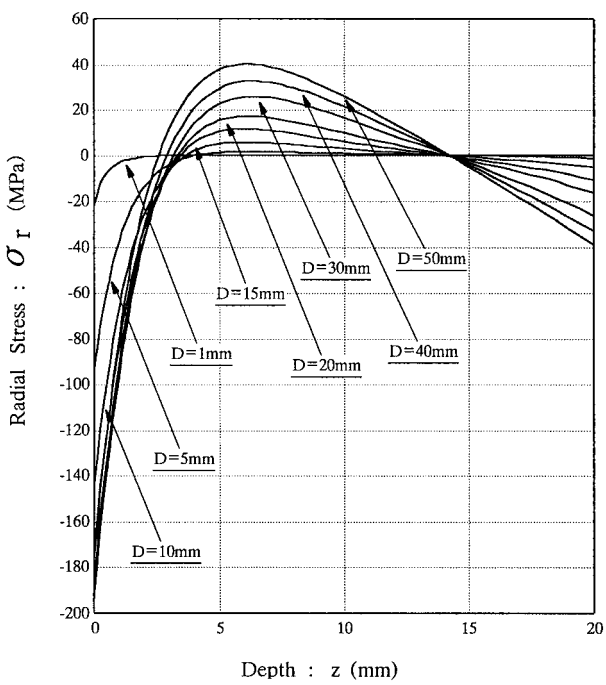

Fig. 9. Radial stress along depth at beam centre.

power 1 kW is irradiated on the surface of the rectangular specimen (50×50 mm, thickness 20×mm) set on the x–y moving table. The four AE (Acoustic Emission) sensors with 200 kHz are put directly under the specimen as shown in Fig. 13 and the fracture signal is detected by them. The experiments are carried out by the repeated irradiations with various laser power densities to obtain the critical P_c. The fracture corresponding to the crack initiation was proved by the SEM observations after sensing the signal with AE analyzer.

Fig. 14 shows the SEM photographs of the fractured specimen with irradiation of $D=5$ mm and $P_c=$ W mm^{-2}. A white circle was the trace of the irradiated

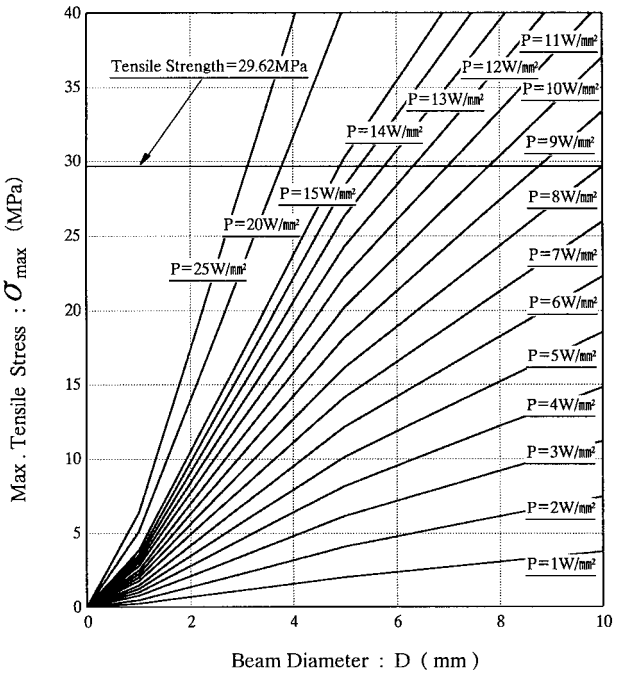

Fig. 10. Maximum tensile stress with beam diameter.

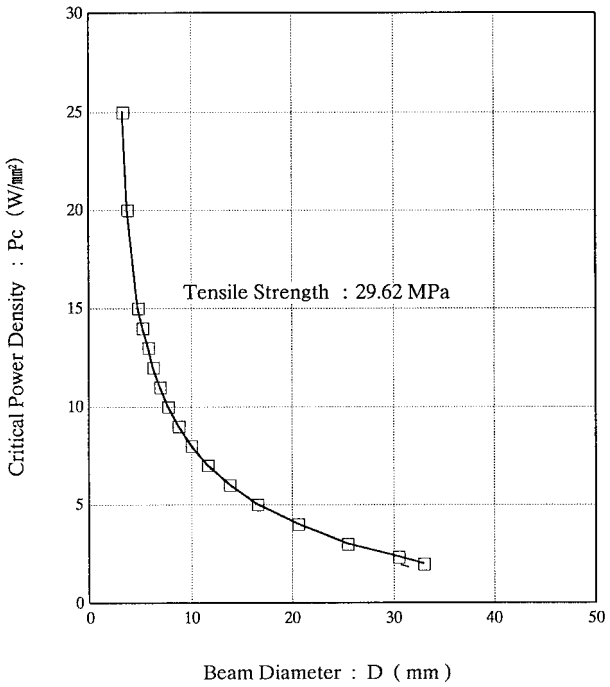

Fig. 11. Critical fracture curve.

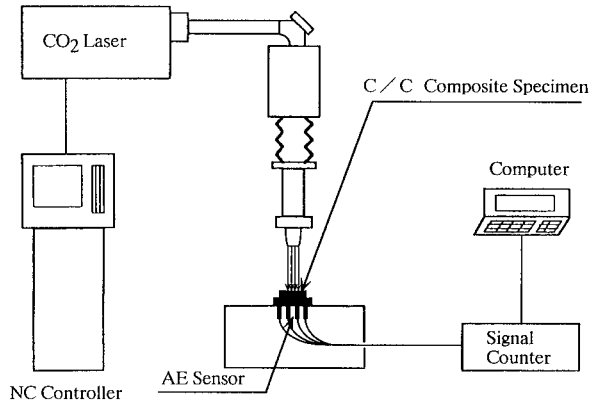

Fig. 12. Experimental apparatus.

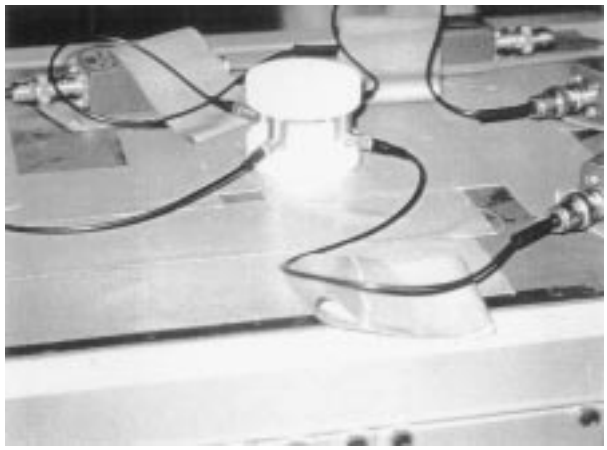

Fig. 13. AE sensing system.

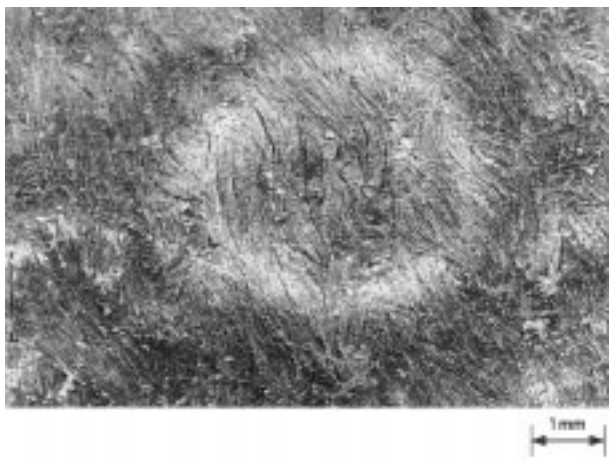

Fig. 14. SEM photograph of fracture surface.

Fig. 15. SEM photograph of fracture surface.

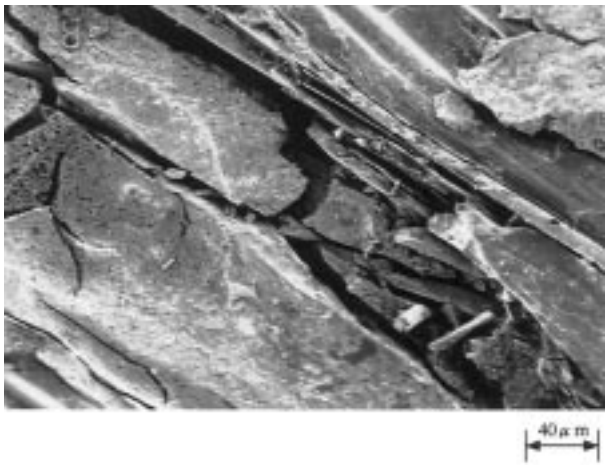

Fig. 16. SEM photograph of fracture surface.

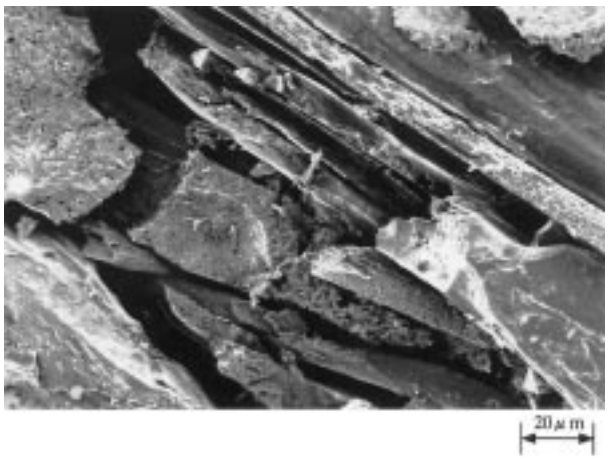

Fig. 17. Magnified SEM photograph of fracture surface.

beam in which and around which the cracks are observed. The magnified photograph inside the region of the laser beam is shown in Fig. 15 where the cracks breaking fibres and running along fibres are confirmed.

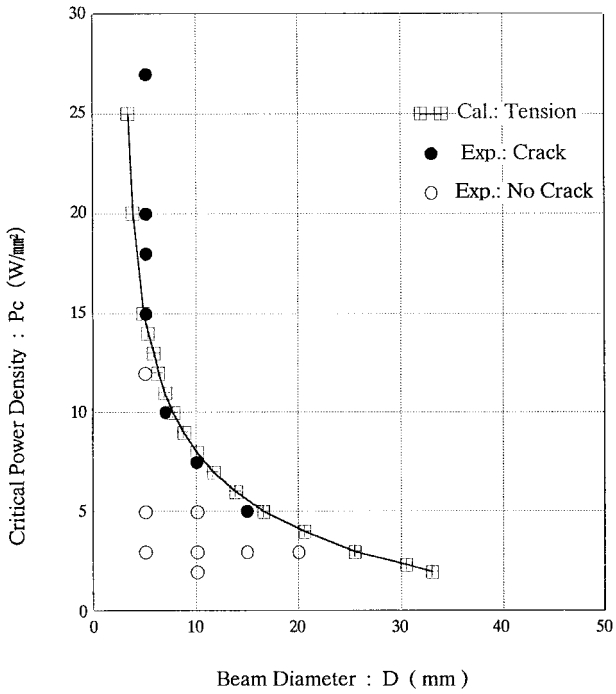

Fig. 18. Experimental results of critical fracture curve.

Fig. 16 displays the cracks in matrix in which spalling occurs. Fig. 17 gives the fracture of the magnified fibres.

The experimentally obtained results are plotted in Fig. 18 where a solid line stands for analytical fracture curve by FEM and solid circles indicate the experimental results. The experimental results agree well with the analytical one. It was concluded that the represented approach was very effective to evaluate thermal shock strength of C/C composite.

7. Conclusions

A simple and more reliable technique than the quenching method was presented to evaluate thermal shock strength of C/C composite. The procedure consists of laser pulse irradiation and sensing AE signals to catch fracture of the materials. The critical fracture curve was derived based on FEM analysis and compared with the laser irradiation experiments. The following conclusions were obtained:

1. The maximum temperature takes place on the irradiated surface at the end of laser pulse.
2. The maximum thermal stress appears on the irradiated surface just outside laser beam.
3. Defining the critical power density P_c of laser beam, which causes the material fracture, the critical fracture curve was constructed for the estimation of thermal shock strength.

4. Using CO_2 laser, thermal shock experiments were done to obtain P_c and the experimental results agree well with the theoretical one.
5. lt was shown that P_c could be a new measure of thermal shock strength.

References

[1] J.R. Strife, J.E. Sheehan, Ceramic coatings for carbon–carbon composites, Ceramic Bulletin 67 (1988) 369–374.

[2] J.D. Buckley, Carbon–carbon; an overview, Ceramic Bulletin 67, (1988) 364–368.

[3] K. Fukuda, Development and applications of three-dimensional weaving. The 676th Lecture by Japan Soc. Mech. Eng., Newest Technology for ACM. Lecture Text, Japanese Society of Mechanical Engineering, 1988, pp. 21–24.

[4] W.C. Chang, C.C. Ma, N.W. Tai, C.B. Chen, Effects of processing methods and parameters on the mechanical properties and microstructure of carbon–carbon composites, Journal Materials Sci., 29, (1994), 5959–5967.

[5] H. Kawata, H. Nakao, S. Hashimoto, H. Hatta, Y. Kogo, Delamination fracture toughness of c/c composite with different layered structures Procd. 3rd Materials & Processing Meeting, Japanese Society of Mechanical Engineering, No. 65–38, 1995, pp. 121–122.

[6] J. Takahashi, J. Watanabe, K. Kenmochi, H. Fukuda, R. Hayashi, Fracture toughness of C/C composite with plane weaving. Procd. 72nd General Meeting, Japanese Society of Mechanical Engineering, No 95–1, 1995, pp. 188–189.

[7] D.P.H. Hasselman, Unified thermal shock fracture initiation and crack propagation in brittle ceramics, Journal of the American Ceramics Society 52, (1969) 600–604.

[8] Jap. Ceram. Soc., Mechanical Characteristics of Ceramics, Jap. Ceram. Soc., Tokyo, 1979, 69–75.

[9] P.F. Becher, D. Lewis III, K.R. Carman, A.C. Gonzalez, Thermal shock resistance of ceramics—size and geometry effects in quench tests, Ceramic Bulletin 59 (1980) 542–545.

[10] T. Ko, N. Nishikawa, M. Hibino, M. Takatsu, Temperature dependent heat transfer coefficient under thermal shock of ceramics, Journal Ceram. Soc. Japan, 101 (1993) 788–792.

[11] T. Sakuma, U. Iwata, Biot-number and thermal stress in quenching process of ceramics, Journal Ceram. Soc. Japan 104 (1996) 743–747.

[12] K.T. Faber, M.D. Huang, Quantitative studies of thermal shock in ceramics based on a novel test technique, Journal of the American Ceramics Society 64 (1981) 296–301.

[13] J. Lamon, D. Pherson, Thermal stress failure of ceramics under repeated rapid heatings, Journal of the American Ceramics Society 74 (1991) 1188–1196.

[14] H. Awaji, M. Ogawa, S. Satoh, New thermal shock test method of ceramics, Transactions of the Japanese Society of Mechanical Engineers, Ser. A 59 (1993) 2941–2946.

[15] M. Takatsu, N. Nishikawa, Maximum thermal stress temperature-dependent thermal conductivity under rapid heating and cooling, Journal of Chemical Engineers 19 (1993) 633–638.

[16] S. Akiyama, S. Amada, A new method to evaluate the thermal shock resistance of ceramics by laser irradiation, Fusion Technology 23, (1993) 426–434.

[17] S. Akiyama, S. Amada, M. Shimada, T. Yoshii, Estimation of thermal shock resistance of $A1_2O_3$ ceramics by laser irradiation, JSME International, Ser. A 38 (1995) 594–600.

[18] S. Akiyama, S. Amada, M. Shimada, T. Senda, T. Yoshii, Thermal shock strength of TiB_2 with different porosity by laser irradiation technique, Transactions of the Japanese Society of Mechanical Engineering 61 (1995) 1896–1901.

[19] Japanese Society of Mechanical Engineering (Eds.), Data Book on Heat Transfers, 4th ed, p. 68, Japanese Society of Mechanical Engineering, Tokyo, 1986.